HHS Public Access

Author manuscript

Mol Pharm. Author manuscript; available in PMC 2020 September 03.

Published in final edited form as:

Mol Pharm. 2019 September 03; 16(9): 3904–3915. doi:10.1021/acs.molpharmaceut.9b00512.

Enhancing the Efficacy of Melanocortin 1 Receptor-Targeted Radiotherapy by Pharmacologically Upregulating the Receptor in Metastatic Melanoma

Mengshi Li[†], **Dijie Liu**[‡], **Dongyoul Lee**[§], **Somya Kapoor**[†], **Katherine N. Gibson-Corley**[‖], **Thomas P. Quinn**[⊥], **Edwin A. Sagastume**[#], **Sarah L. Mott**[¶], **Susan A. Walsh**[†], **Michael R. Acevedo**[†], **Frances L. Johnson**[#,▽], **Michael K. Schultz**[*,†,‡,§,#,¶]

[†]Department of Radiology, University of Iowa, Iowa City, Iowa 52242, United States

[‡]Department of Pediatrics, University of Iowa, Iowa City, Iowa 52242, United States

[§]Human Toxicology Program, University of Iowa, Iowa City, Iowa 52242, United States

[‖]Department of Pathology, University of Iowa, Iowa City, Iowa 52242, United States

[¶]Holden Comprehensive Cancer Center, University of Iowa, Iowa City, Iowa 52242, United States

[▽]Department of Internal Medicine, University of Iowa, Iowa City, Iowa 52242, United States

[⊥]Department of Biochemistry, University of Missouri, Columbia, Missouri 65211, United States

[#]Viewpoint Molecular Targeting, Inc., Coralville, Iowa 52241, United States

Abstract

Melanocortin 1 receptor (MC1R) is under investigation as a target for drug delivery for metastatic melanoma therapy and imaging. The purpose of this study was to determine the potential of using BRAF inhibitors ($BRAF_i$) and histone deacetylase inhibitors ($HDAC_i$) to enhance the delivery of MC1R-targeted radiolabeled peptide ([^{212}Pb]DOTA-MC1L) by pharmacologically upregulating the MC1R expression in metastatic melanoma cells and tumors. MC1R expression was analyzed in de-identified melanoma biopsies by immunohistochemical staining. Upregulation of MC1R expression was determined in $BRAF^{V600E}$ cells (A2058) and BRAF wild-type melanoma cells (MEWO) by quantitative real-time polymerase chain reaction, flow cytometry, and receptor-ligand binding assays. The role of microphthalmia-associated transcription factor (MITF) in the upregulation of MC1R was also examined in A2058 and MEWO cells. The effectiveness of [^{212}Pb]DOTA-MC1L α-particle radiotherapy in combination with $BRAF_i$ and/or $HDAC_i$ was

[*]**Corresponding Author**: michael-schultz@uiowa.edu. Phone: +1 (319) 335-8017.

Author Contributions

M.L. contributed to the design and undertaking of experiments and preparation of the manuscript; D. Liu and D. Lee contributed to the undertaking of animal experiments; S.K. contributed to the undertaking of key in vitro experiments; K.N.G.-C. contributed to the pathology analysis; T.P.Q. contributed to the evaluation of results and editing the manuscript; E.A.S. contributed to the undertaking of animal experiments; S.L.M. provided statistical evaluation of results; S.A.W. and M.R.A. contributed to the experimental imaging design and evaluation of image results; F.L.J. contributed to the experimental design, evaluation of results, and writing/editing the manuscript; M.K.S. contributed to the experimental design, evaluation of results, and writing/editing the manuscript.

The authors declare the following competing financial interest(s): This paper consists of original research and has not been submitted for publication in another journal. MKS, FLJ, and EAS disclose interest in Viewpoint Molecular Targeting, Inc., which has potential financial interest in this work.

determined in athymic nu/nu mice bearing A2058 and MEWO human melanoma xenografts. High expression of MC1R was observed in situ in clinical melanoma biopsies. $BRAF_i$ and $HDAC_i$ significantly increased the MC1R expression (up to 10-fold in mRNA and 4-fold in protein levels) via MITF-dependent pathways, and this increase led to enhanced ligand binding on the cell surface. Inhibition of MITF expression antagonized the upregulation of MC1R in both $BRAF^{V600E}$ and $BRAF^{WT}$ cells. Combining [^{212}Pb]DOTA-MC1L with $BRAF_i$ and/or $HDAC_i$ improved the tumor response by increasing the delivery of ^{212}Pb α-particle emissions to melanoma tumors via augmented MC1R expression. These data suggest that FDA-approved $HDAC_i$ and $BRAF_i$ could improve the effectiveness of MC1R-targeted therapies by enhancing drug delivery via upregulated MC1R.

Graphical Abstract

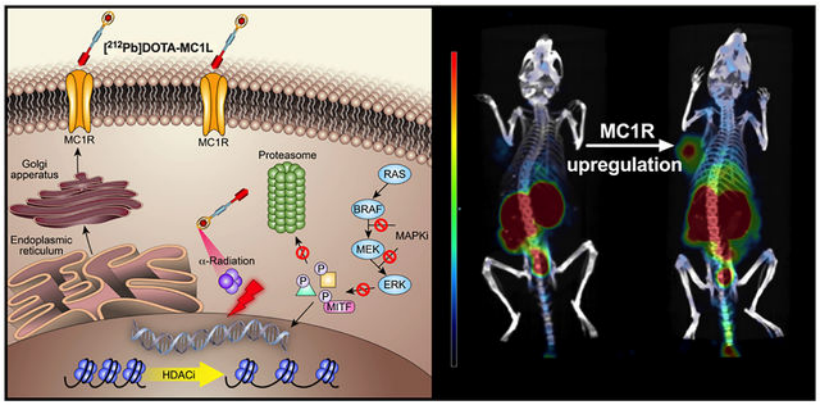

Keywords

melanoma; melanocortin 1 receptor; radionuclide therapy; histone deacetylase inhibitors; MAPK pathway inhibitors; BRAF inhibitors; MEK inhibitors

INTRODUCTION

Metastatic melanoma is a lethal form of skin cancer and is one of the fastest growing incidences in the world.[1] Recent breakthrough checkpoint-inhibitor immunotherapies and inhibitors of mitogen-activated protein kinase (MAPK) pathway (including BRAF and MEK inhibitors) have significantly improved the outcomes,[2–4] but low response rates,[5–8] acquired drug resistance,[9–17] and serious side effects[18–21] remain serious challenges to further improvements in the outcomes for patients with late-stage metastatic melanoma (5 year survival < 25%).[1] Melanocortin subtype 1 receptor (MC1R) is a seven-transmembrane G-protein coupled receptor that has been investigated as a potential target for drug delivery for melanoma therapy because of its high expression in malignant melanoma versus normal organs and tissues.[22–26] One particularly promising avenue for introduction of MC1R-targeted therapy is the use of radiolabeled analogues of the native-cognate peptide ligand of MC1R (i.e., α-melanocyte-stimulating hormone; α-MSH). Numerous radiolabeled α-MSH analogues have been developed that bind to MC1R with high specificity and affinity.[27–34] However, reports of the utility of these ligands have been largely restricted to the use of B16

murine melanoma models that has an extraordinarily high MC1R expression (8000−9000 MC1R receptors/cell).[25,35] In contrast, the MC1R expression in human melanoma cell lines and tumors appears to be more heterogeneous.[23–25]

In this study, we investigated an approach to improving the MC1R-mediated delivery of drug payload by pharmacological upregulation of the receptor expression in human melanoma. Natively, MC1R expression is responsive to external stimuli, including ultraviolet-induced DNA damage and exogenous molecular factors in the microenvironment proximal to cells via α-MSH, ACTH, bFGF, and ET-1 signaling.[22,36–39] In this study, we have focused on two types of Food and Drug Administration (FDA)-approved pharmacological agents to upregulate MC1R in human melanoma cells (i.e., BRAF inhibitors and HDAC inhibitors). Previous studies have shown that MAPK inhibition can induce robust upregulation of melanosomal antigens,[40] some of which have been studied as potential targets for drug delivery to melanoma. For example, MAPK inhibition upregulated glycoprotein Nmb and endothelin subtype B receptors in melanoma cells and improved the delivery of antibody drug conjugates via these targets.[41,42] Similarly, epigenetic modulators, such as histone deacetylase inhibitors ($HDAC_i$) vorinostat (Zolinza) increased the expression of cell-surface norepinephrine transporters in neuroblastoma, leading to enhanced efficacy of tumor-antigen-targeted therapies.[43–45] In light of these findings, we aimed to explore the potential of improving the delivery of radiolabeled α-MSH analogues to melanoma by upregulating the MC1R expression in human melanoma cells. MC1R gene expression is controlled in part by microphthalmia-associated transcription factor (MITF),[22,37,46,47] a master-regulator transcription factor of pigmentation and melanoma cell proliferation.[48–50] Thus, as part of the investigation, we sought to further explore the role of MITF in MC1R upregulation arising from pharmacological treatments.

In this study, we present pharmacological approaches to upregulating MC1R expression in human melanoma cell lines and tumors by $BRAF_i$ and $HDAC_i$ via MITF-dependent mechanisms. The combination of $BRAF_i$, $HDAC_i$, and MC1R-targeted α-particle radiotherapy using radiolabeled peptide [^{212}Pb]DOTA-MC1L significantly improved survival outcomes in mice bearing human melanoma tumors ($BRAF^{V600E}$ A2058, $BRAF^{WT}$ MEWO), despite relatively lower MC1R baseline expression compared to B16 mouse melanoma models.

MATERIALS AND METHODS

Cell Culture and Reagents.

Human melanoma cell lines used for this study included BRAF-mutant ($BRAF^{V600E}$) A2058 and BRAF wild-type ($BRAF^{WT}$) MEWO cells obtained from American Type Culture Collection, and they were used within 15 passages for all experiments. A2058 cells were maintained in Dulbecco's modified Eagle's medium (DMEM) with 10% fetal bovine serum (FBS), 100 units mL^{-1} penicillin, and 100 units mL^{-1} streptomycin. MEWO cells were cultured in DMEM/F-12 1:1 media supplemented with 10% FBS, 100 units mL^{-1} penicillin, and 100 units mL^{-1} streptomycin. All cells were grown at 37 °C in a humidified atmosphere (5% CO_2). Drugs used in this study were purchased commercially, including $BRAF_i$ dabrafenib and vemurafenib (Selleckchem) for MAPK inhibition and $HDAC_i$ vorinostat

(Selleckchem) and 4-phenylbutyrate (Sigma-Aldrich). ^{203}Pb chloride was obtained from Lantheus Medical Imaging (North Billerica, MA). ^{224}Ra/^{212}Pb generator was provided by Oak Ridge National Laboratory (Oak Ridge, TN). Pb-specific resin was obtained from Eichrom Technologies (Lisle, IL).

Immunohistochemical Analysis of MC1R in Clinical Melanoma Sections.

Paraffinized clinical melanoma biopsy sections were provided by the Tissue Procurement Core Facility at the University of Iowa. MC1R expression in representative clinical melanoma samples from early stage T1 to late stage T4 ($n = 6$) was analyzed by immunohistochemical (IHC) staining. Briefly, samples were deparaffinized by three cycles of 100% xylene (3 min cycle^{-1}), two cycles of 100% ethanol (3 min cycle^{-1}), one cycle of 95% ethanol (1 min), and one cycle of 70% ethanol (1 min). Antigen retrieval was performed in 10 mM citrate buffer (pH = 6) at 95 °C for 15 min. The sections were blocked in 5% horse serum (Sigma, H1046) for 1 h, followed by incubation with rabbit monoclonal anti-MC1R (1:100 dilution, ab125031, Abcam) at 4 °C overnight. Secondary antibody incubation used HRP goat anti-rabbit IgG antibody-peroxidase (PI-1000–1, Vector Labs). The samples were finally stained with ImmPACT NovaRED Peroxidase (HRP) Substrate (SK-4805, Vector Labs). Bright-field microscopy was performed using an Olympus BX-61 instrument in the Central Microscopy Research Facility at the University of Iowa.

Quantitative Real-Time PCR for MC1R Gene Expression.

A2058 (BRAF^{V600E}) cells were treated with BRAF$_i$ dabrafenib (2−10 μM) and HDAC$_i$ 4-phenylbutyrate (2−10 mM) for 24 h. MEWO (BRAF^{WT}) cells were exposed to HDAC$_i$ 4-phenylbutyrate (2−10 mM) and vorinostat (2−10 μM) for 24 h. BRAF^{WT} cells were not treated with BRAF$_i$ because BRAF$_i$ is not indicated for melanoma patients who are not positive for BRAF^{V600E} mutation. Total RNA was isolated using an RNeasy Mini Kit (74104, Qiagen) according to the manufacturer's protocol. cDNA samples were collected from 1 μg of total RNA using a High Capacity cDNA Reverse Transcription Kit (4368814, Applied Biosystem). Upon assay, 20 ng of cDNA template was used for quantitative real-time polymerase chain reaction (qRT-PCR) using the Taqman Gene Expression Assay for human MC1R (assay ID: Hs00267167_s1, Thermo Fisher Scientific). Human 18S (assay ID: Hs99999901_s1) and glyceraldehyde 3-phosphate dehydrogenase (GAPDH) (assay ID: Hs03929097_g1, Thermo Fisher Scientific) were applied as internal housekeeping gene controls. The qRT-PCR reaction was performed using the Taqman Fast Universal Master Mix (435 2042, Applied Biosystem) in 96-well reaction plates on an Applied Biosystem 7900HT at the Genomic Division at the University of Iowa. Relative MC1R mRNA level versus control was calculated by the comparative $\Delta\Delta C_t$ method.

Flow Cytometry Analysis of Cell Surface MC1R Protein Density.

A2058 cells were incubated with BRAF$_i$ (2 μM dabrafenib or 5 μM vemurafenib) and HDAC$_i$ (2 mM 4-phenylbutyrate or 2 μM vorinostat) for 24 h. BRAF^{WT} cells (MEWO) were exposed to HDAC$_i$ (4-phenylbutyrate and vorinostat) for 24 h. Cell surface MC1R expression was then determined in melanoma cells by flow cytometry. Upon assay, the cells were resuspended in 100 μL of ice-cold phosphate buffered saline (PBS) with 1% bovine serum albumin (BSA), containing 0.3 μg of R-phycoerythrin (R-PE)-conjugated anti-MC1R

rabbit polyclonal IgG antibody (sc-6875, Santa Cruz Biotech). R-PE-anti-MC1R antibody was prepared using a Lightning-Link HRP Conjugation Kit (703−0000, Innova Biosciences) according to the manufacturer's protocol. The isotype background was determined using R-PE-conjugated isotype-control (ab172730, Abcam). Cells were incubated with R-PE-conjugated antibodies for 20−30 min on ice and washed with ice-cold PBS with 1% BSA. The samples were analyzed using a Becton Dickinson LSR flow cytometer (BD Biosciences) in the Flow Cytometry Facility at the University of Iowa. Data were analyzed using FlowJo software (V9; Tree Star, Inc.).

MC1R Receptor Binding with [^{125}I]-Nle^{4}-D-Phe^{7}-α-MSH.

MAPK and HDAC activity were inhibited by $BRAF_i$ (1−10 μM dabrafenib) and $HDAC_i$ (0.5−10 mM 4-phenylbutyrate), respectively, in A2058 cells. For MEWO cells, HDAC activity was inhibited by incubation with 4-phenylbutyrate (0.5−10 mM) and vorinostat (0.5−10 μM). Treatments were carried out for 12−24 h in flat-bottom polystryene 24-well plates. MC1R-radioligand binding assays were conducted using synthetic-radiolabeled α-MSH analogue [^{125}I]-Nle^{4}-D-Phe^{7}-α-MSH ([^{125}I]-NDP-α-MSH, NEX352010UC, PerkinElmer). Briefly, cell culture media containing the drugs were aspirated, followed by a gentle wash with 0.5 mL of binding media (modified Eagle's medium with 25 mM *N*-(2-hydroxyethyl)piperazine-*N*′-ethanesulfonic acid, 0.2% BSA, and 0.3 mM 1,10-phenanthroline). Binding media (0.3 mL) containing ~20 000 cpm [^{125}I]-NDP-α-MSH were added to cells and incubated for 2 h at 25 °C. Following the radioligand binding, the cells were rinsed gently twice with0.5 mL of ice-cold 10 mM PBS buffer with 0.2% BSA and lysed in 0.5 mL of 0.5 M NaOH for 5 min. Cell lyses were harvested, and radioactivity was measured using standard gamma counting (Packard Cobra 5002, PerkinElmer).

Immunoblotting of MC1R and MITF.

Total protein was extracted with RIPA buffer (R0278, Sigma-Aldrich) containing protease inhibitor (04693159001 Roche, Sigma-Aldrich). Each protein sample (10 μg) was loaded onto 4–15PCT Mini-Protean TGX Precast Gel (4561094, BioRad) and developed in Tris buffered-saline Tween 20 (1706435, Bio Rad). The protein samples were then transferred to 0.2 μm polyvinylidene fluoride (PVDF) membranes (1620176, Bio Rad) in 1× Nu-PAGE transfer buffer (NP00061, Life Technologies). After blocking in 5% BSA for 2 h, the PVDF membranes were incubated with rabbit monoclonal anti-MC1R (1:1000 dilution, ab125031, Abcam), rabbit monoclonal anti-MITF (1:1000 dilution, ab140606, Abcam), rabbit monoclonal anti-p-ERK (1:1000 dilution, #8544, Cell Signaling Technology), and rabbit monoclonal anti-vinculin antibody (1:10000 dilution, ab129002, Abcam) at 4 °C overnight. Secondary antibody incubation employed goat anti-rabbit IgG H&L (1:10000, ab97051, Abcam) at room temperature for 1 h. Membranes were soaked in West Pico Supersignal Chemiluminescent Substrate (37070, ThermoFisher Scientific) for 5 min before imaging. All assays were conducted in at least duplicate to confirm the results.

MITF expression was attenuated in A2058 and MEWO cells using a predesigned *MITF* dicer-substrate siRNA kit (TriFECTa DsiRNA Kit) (hs.Ri.MITF.13, Integrated DNA Technologies). Briefly, *MITF* Dsi-RNA was diluted with Opti-MEM in six-well tissue culture plates. Lipofectamine RNAiMAX was also diluted with Opti-MEM and added to the

MITF Dsi-RNA solution. The complex solution was mixed gently at room temperature for 20 min. The cells were suspended in complete growth media without antibiotics and added to the complex solution to make the final *MITF* Dsi-RNA concentration 20 nM. The cells were then cultured under normal conditions for 2 days. After attenuation of MITF expression, the cells were treated with $BRAF_i$ and $HDAC_i$ to determine the effect of reduced MITF level on MC1R.

Radiosynthesis of [$^{203/212}$Pb]DOTA-MC1L.

MC1R-targeted peptide DOTA-MC1L, a previously-reported ee-cyclized α-MSH analogue conjugated to the DOTA chelator[30–32] (Figure 1), was radiolabeled with ^{203}Pb (E_γ = 279 keV; $t_{1/2}$ = 52 h) for single-photon emission computed tomography (SPECT) imaging and ^{212}Pb ($t_{1/2}$ = 10.6 h) for α-particle radiotherapy, as previously described.[51] Briefly, $^{203}PbCl_2$ was dissolved in 0.5 M HCl and $^{212}PbCl_2$ eluted from ^{224}Ra/^{212}Pb generator (US Department of Energy, Oak Ridge, TN USA) using 2 M HCl. $^{203}PbCl_2$ and $^{212}PbCl_2$ solutions were further purified by column chromatography as we described previously[51] using 50 mg of Pb-specific resin to remove metallic contaminants and decay products. Purified ^{203}Pb or ^{212}Pb was obtained by elution from the Pb-specific resin using 2 mL of 0.5 M NaOAC buffer (pH = 6). Following purification, $^{203}Pb^{2+}$ or $^{212}Pb^{2+}$ solutions (~370 MBq) were buffered to pH = 5.4 and reacted with 20 nmol of DOTA-MC1L at 80 °C for 30 min. The resulting [$^{203/212}$Pb]DOTA-MC1L radiolabeled conjugates were further purified from excess unlabeled DOTA-MC1L to single species on an Agilent 1100 RP-HPLC system using a linear gradient of 16−26% acetonitrile over 20 min in 20 mM HCl on the Vydac 218TP C18 column (4.6 × 150 mm, 5 μm) with 1 mL min^{-1} flow rate. Acetonitrile and HCl were removed by Strata-X reverse-phase extraction (Phenomenex, Torrance, CA).

Upregulation of MC1R and in Vivo α-Particle Radiotherapy.

All animal studies were performed in accordance with the Guide for the Care and Use of Laboratory Animals, according to protocols approved by the University of Iowa Animal Care and Use Committee. A2058 melanoma xenografts were developed in female athymic nu/nu mice (Envigo) by subcutaneous inoculation of 5 × 10^6 A2058 melanoma cells with 50% Matrigel (354234, CORNING) in total growth media near the left shoulder. Upregulation of MC1R in vivo was initially analyzed by MC1R−IHC staining. When the tumor size neared 100 mm^3, the animals were administrated with $BRAF_i$ vemurafenib (10 mg kg^{-1}; p.o.; b.i.d.) and $HDAC_i$ 4-phenylbutyrate (90 mg kg^{-1}; i.p.; q.d.) for 7 days (n = 2). A2058 tumors were collected and fixed in 4% paraformaldehyde for 48 h before being embedded in paraffin. MC1R−IHC staining was then performed as described above.

SPECT/CT imaging was performed in athymic nu/nu mice bearing A2058 melanoma xenografts using [^{203}Pb]DOTA-MC1L at the University of Iowa Small Animal Imaging Core. When the tumor size reached 200 mm^3, the animals were treated with vemurafenib (10 mg kg^{-1}, p.o.) and 4-phenylbutyrate (90 mg kg^{-1}, i.p.) 6 h prior to imaging studies. [^{203}Pb]DOTA-MC1L [13.05 MBq (±0.1 MBq)] (molar activity of 70 MBq $nmol^{-1}$ peptide) was injected via tail vein in the anesthetized mice. Two hours post injection, SPECT imaging was performed while the mice were under isoflurane anesthesia (2%) using an INVEON trimodality SPECT/positron emission tomography/computed tomography (CT)

scanner (Siemens Preclinical, Knoxville, TN) equipped with medium-energy (0.3 mm) pinhole collimators 40 mm from the center of field of view. SPECT images were generated by acquiring 60 20 s projections over a total of 1.5 gantry rotations with 60 mm of bed travel. Data was reconstructed using 3D-OSEM algorithm with eight iterations and six subsets. A CT image was acquired for anatomical coregistration purposes. Post-reconstruction images were smoothed with a three-dimensional Gaussian kernel. Animals were euthanized at the conclusion of the imaging, and a postimaging biodistribution analysis was performed. Briefly, the tumors and organs of interest were collected and weighed. Radioactivity was measured by a Packard Cobra II Gamma Counter (PerkinElmer).

MC1R-targeted α-particle radiotherapy was conducted in female athymic nu/nu mice bearing A2058 melanoma xenografts ($n = 10$) using the 212Pb-labeled therapeutic counterpart [^{212}Pb]DOTA-MC1L. All therapies were initiated on day 0, when the A2058 tumor size was 85 ± 18 mm^3. For [^{212}Pb]DOTA-MC1L as a monotherapy, a single dose of 5.2 MBq [^{212}Pb]DOTA-MC1L was injected (100 μL of saline) via the tail vein. The dose of [^{212}Pb]DOTA-MC1L was selected based on previously published dose-escalating studies.[31] Combination therapies included a single dose of [^{212}Pb]-DOTA-MC1L injected (i.v.) at 6 h after administration of vemurafenib (10 mg kg^{-1}, p.o.) and 4-phenylbutyrate (90 mg kg^{-1}, i.p.), followed by daily treatments of vemurafenib (10 mg kg^{-1}, p.o., b.i.d.) and 4-phenylbutyrate (90 mg kg^{-1}, i.p., q.d.) for 30 days. At the conclusion of the study, dose-limiting organs (i.e., kidney) were harvested from the surviving animals for hemotoxylin and eosin (H&E) analysis in the Comparative Pathology Laboratory at The University of Iowa.

The combination of [^{212}Pb]DOTA-MC1L and HDAC$_i$ 4-phenylbutyrate was also confirmed in female athymic nu/nu mice bearing BRAF^{WT} MEWO melanoma xenografts ($n = 6$−7), developed by subcutaneous injection of 5 × 10^6 cells with 50% Corning Matrigel near the left shoulder. All therapies were initiated on day 0 (tumor size was 47 ± 5 mm^3). A single dose of 5.2 MBq [^{212}Pb]DOTA-MC1L was introduced at 6 h after 4-phenylbutyrate (90 mg kg^{-1}, i.p.), followed by daily treatment with 4-phenylbutyrate (90 mg kg^{-1}, i.p., q.d.) for 30 days. Body weight and animal wellness were monitored on a daily basis. The tumor size was measured twice per week in each animal and calculated using the length × width formula: ($L \times W^2$)/2. Animals were removed from the study when the tumor size reached 1500 mm^3, tumor ulcerations appeared, body weight loss was more than 20% compared with starting weight, or other significant toxicity was observed.

Statistical Analysis.

Tumor growth statistical analysis was performed by the Biostatistics Core in the Holden Comprehensive Cancer Center at the University of Iowa. A two-tailed Student t-test was employed to analyzed significant differences in observations. Linear mixed-effects regression models were used to estimate and compare treatment group-specific tumor growth curves. Pairwise comparisons were performed to identify treatment group differences in the growth curves. The Kaplan−Meier method was used to estimate survival curves, and group comparisons were made using log rank tests. In addition to longer-term growth rate analyses, a single-point comparison analysis of tumor size was conducted on the date that the first control animals were to be euthanized to allow statistical comparison of group-

specific tumor growth. All tests were two-sided and carried out at the 5% significance level using SAS v9.4 software (SAS Institute, Cary, NC).

RESULTS

Mixed Levels of MC1R Expression Are Found in Clinical Melanoma Biopsy Samples.

To investigate the expression of MC1R in situ in melanoma tumors, a pilot study was performed using de-identified melanoma biopsy samples from stage 1b to 4b ($n = 6$). The specimens were analyzed using MC1R IHC staining. In these clinical samples, mixed levels of MC1R expression were observed (Figure 2). All melanoma samples demonstrated positive immunoreactivity against MC1R, but clearly higher MC1R staining was observed in tumor cells from later stage melanoma tumors (patient 3 and patient 4) as compared to earlier stage tumors (patient 1 and 2). The MC1R expression was found to be highly localized in melanoma lesion (arrows) but largely absent in the adjacent normal tissue. Interestingly, considerable MC1R protein appeared to be cytosolic in localization compared to the cell surface expression.

MC1R Expression Can Be Upregulated by BRAF and HDAC Inhibitors.

The efficacy of this MC1R-targeted therapy is largely dependent on the density of MC1R on the surface of melanoma cells. Initial experiments showed that *MC1R* mRNA was significantly upregulated (8- to 10-fold) in $BRAF^{V600E}$ melanoma A2058 cells upon inhibition of MAPK by dabrafenib and HDAC inhibition by 4-phenylbutyrate (Figure 3A). Similarly, after treatment with $HDAC_i$, *MC1R* mRNA levels were found to be significantly enhanced (6- to 8-fold) in $BRAF^{WT}$ MEWO cells (Figure 3A). To determine if increased levels of mRNA expression conveyed an increase in the cell surface receptor density, flow cytometry assays were performed in these melanoma cell lines with an expanded set of drugs. In $BRAF^{V600E}$ A2058 cells, 24 h treatment with $BRAF_i$ (dabrafenib and vemurafenib) and $HDAC_i$ (4-phenylbutyrate and vorinostat) robustly induced MC1R expression up to 2- to 3-fold (Figure 3B). Because $BRAF_i$ is not indicated for patients whose melanoma has not acquired the $BRAF^{V600E}$ mutation, $BRAF_i$ was not applied to $BRAF^{WT}$ MEWO cells. Instead, HDAC inhibition using 4-phenylbutyrate and vorinostat augmented the expression of MC1R up to 2-fold in cells (Figure 3B), indicating that HDAC inhibition has the potential of bypassing MAPK signaling alterations and triggering the upregulation of MC1R expression epigenetically.

Enhanced [^{125}I]-NDP-α-MSH binding with MC1R was observed following a dose- and time-dependent manner in both $BRAF^{V600E}$ and $BRAF^{WT}$ cells. In A0258 cells, $BRAF_i$ dabrafenib increased [^{125}I]-NDP-α-MSH binding by 2- to 3-fold at 12−24 h after treatments were initiated. Similarly, the highest [^{125}I]-NDP-α-MSH binding (5-fold increase) was observed after treatment with 10 mM $HDAC_i$ 4-phenylbutyrate for 24 h (Figure 3C). In MEWO cells, a similar dose- and time-dependent upregulation of MC1R was observed after exposure to $HDAC_i$ vorinostat and 4-phenylbutyrate, with about a 3-fold increase in [^{125}I]-NDP-α-MSH binding after 24 h treatment. These data support the hypothesis that MAPK and HDAC inhibition can increase the density of functional MC1R binding sites on the cell-surface membrane of melanoma cells that are available for the α-MSH analogue to bind.

MC1R Upregulation Is Mediated by MITF.

MITF has been extensively investigated in melanoma for regulation of melanosomal antigen expression, melanoma cell proliferation, and as part of melanoma cell-survival mechanisms that arise in response to therapies.[49,50,52,53] Here, using *MITF* gene-silencing methods, we sought to determine if the observed MC1R upregulation in response to BRAF and HDAC inhibitors depended on the MITF signaling pathway. We found that the MITF expression was upregulated in parallel with MC1R upon treatments in A2058 and MEWO cells (Figure 4A,B). In A2058 cells, $BRAF_i$ dabrafenib and $HDAC_i$ vorinostat significantly induced MITF and MC1R protein expression (Figure 4A, first two lanes). Concordantly, in MEWO cells, similar responses were observed upon HDAC inhibition using vorinostat and 4-phenylbutyrate (Figure 4B, first two lanes). In $BRAF^{V600E}$ A2058 cells, treatment of $BRAF_i$ dabrafenib largely reduced the p-ERK expression. Interestingly, exposure to $HDAC_i$ vorinostat also compromised the expression of phospho-ERK1/2 in A2058 cells, as indicated by the immunoblotting (Figure 4A, lane 3), whereas in $BRAF^{WT}$ MEWO cells, 4-phenylbutyrate did not affect the MAPK activity, but vorinostat slightly decreased the p-ERK expression.

To determine if MITF was required for enhanced MC1R expression, melanoma cells were incubated with a predesigned *MITF* DsiRNA. Compared with the scrambled Dsi-RNA negative control gene, MITF DsiRNA efficiently inhibited the expression of MITF in both A2058 and MEWO cells (Figure 4C,D). In these cases, we also found that, as MITF was attenuated, MC1R protein levels also were significantly reduced (Figure 4C,D, first lane). Following the attenuation of MITF expression, melanoma cells were further treated with MC1R-upregulating drugs (1 μM dabrafenib or 1 μM vorinostat). We found that the ability of BRAF and HDAC inhibitors to promote the upregulation of MC1R was significantly diminished (Figure 4C,D), indicating that the transcription factor MITF plays an essential role in regulating the MC1R expression in response to MAPK and HDAC inhibition in both $BRAF^{V600E}$ and $BRAF^{WT}$ melanoma cells.

Upregulation of MC1R Enhances ^{212}Pb α-Particle Radiotherapy for Melanoma.

The potential of employing $HDAC_i$ and $BRAF_i$ as a means to enhance the delivery of radiation dose to melanoma was initially examined in $BRAF^{V600E}$ A2058 melanoma xenografts. Vemurafenib and 4-phenylbutyrate were selected as $BRAF_i$ and $HDAC_i$ in in vivo studies based on in vitro findings (Figure 3B). IHC staining of MC1R in A2058 xenografts demonstrated increased MC1R immunoreactivity in melanoma cells upon treatments as compared to control (Figure 5A). SPECT/CT imaging of A2058 melanoma (identified as “T”; Figure 5B) demonstrated a significantly enhanced MC1R expression and accumulation of [^{203}Pb]DOTA-MC1L imaging tracer in the xenograft tumor when the animal was treated with vemurafenib and 4-phenylbutyrate. Residual [^{203}Pb]DOTA-MC1L imaging tracer was excreted rapidly, primarily via kidney and bladder (identified as “K” and “B”). Follow-up biodistribution analysis indicated that the accumulation of [^{203}Pb]DOTA-MC1L in the A2058 tumor (radioactivity/g of tissue) was enhanced 2.2-fold in vemurafenib/4-phenylbutyrate-treated mice versus control. [^{203}Pb]DOTA-MC1L in the tumor/organ ratio (i.e. tumor/blood, skin, kidney, muscle) was enhanced 1.3- to 2.4-fold,

indicating that MC1R upregulation was primarily localized within the melanoma but not in normal tissues.

In athymic nu/nu mice bearing A2058 xenografts, control vehicle-treated animals reached the tumor volume near or greater than 1500 mm^3 as early as day 10 after tumor cell implants (Figure 5C). Meanwhile, limited control of tumor growth was observed in animals treated with vemurafenib and 4-phenylbutyrate (Figure 5C). On the other hand, a single dose of 5.2 MBq [^{212}Pb]DOTA-MC1L induced a significant delay in the tumor growth (**$p < 0.01$ ^{212}Pb vs control; **$p < 0.01$ ^{212}Pb vs Vem; Figure 5C), with the mean tumor volume 247 mm^3 on day 10. More robust arrest of tumor growth was observed when [^{212}Pb]DOTA-MC1L was combined with vemurafenib and 4-phenylbutyrate compared to [^{212}Pb]-DOTA-MC1L monotherapy (*$p < 0.05$ ^{212}Pb/Vem vs ^{212}Pb; *$p < 0.05$ ^{212}Pb/Vem/PBA vs ^{212}Pb). When the control animals approached the tumor volume of 1500 mm^3, the mean tumor size was 166 and 86 mm^3 in ^{212}Pb/Vem and ^{212}Pb/Vem/PBA, respectively (*$p < 0.05$ ^{212}Pb/Vem/PBA vs ^{212}Pb/Vem; Figure 5C). Individual tumor growth was then monitored in each animal cohort for about 100 days. [^{212}Pb]DOTA-MC1L monotherapy significantly suppressed tumor progression compared with controls and nonradiotherapy treatment groups; further, tumor growth suppression was observed when [^{212}Pb]DOTA-MC1L was combined with vemurafenib and 4-phenylbutyrate (Figure 5D). As demonstrated in fractional survival curves, because of the aggressiveness of A2058 melanoma cells, the median overall survival (MOS) was only 11 days in vehicle-treated animals (Figure 5D). Improvement in survival was observed in animals treated with a single dose of [^{212}Pb]DOTA-MC1L (MOS 26 days; ****$p < 0.0001$ ^{212}Pb vs control; ****$p < 0.0001$ ^{212}Pb vs Vem). A combination of vemurafenib and [^{212}Pb]DOTA-MC1L enhanced the delivery of α-particle radiation to the tumor microenvironment via upregulated MC1R and significantly improved the MOS to 34 days (**$p < 0.01$ ^{212}Pb/Vem vs ^{212}Pb; Figure 5D). Adding both vemurafenib and 4-phenylbutyrate to [^{212}Pb]DOTA-MC1L further extended the MOS to 48 days (**$p < 0.01$ ^{212}Pb/Vem/PBA vs ^{212}Pb/Vem; Figure 5D)—representing a nearly 5-fold improvement relative to untreated control animals.

We further tested the combination of [^{212}Pb]DOTA-MC1L and $HDAC_i$ 4-phenylbutyrate in $BRAF^{WT}$ MEWO melanoma xenografts. On the basis of the tumor growth data presented here, MEWO melanoma tumors appeared to be less aggressive than A2058 tumors. Control vehicle-treated animals approached the study endpoint (tumor volume 1500 mm^3) as early as day 41 following initiation of therapies, with the mean tumor volume of 1191 ± 119 mm^3 on day 41 (Figure 6A). In comparison, the combination of [^{212}Pb]DOTA-MC1L and 4-phenylbutyrate arrested tumor growth within the same time frame, and the tumor volume was 225 ± 85 mm^3 (**$p < 0.01$ ^{212}Pb/PBA vs control; Figure 6A). A 52 day MOS was observed in control vehicle-treated animals (Figure 6B). Treatment with 5.2 MBq [^{212}Pb]DOTA-MC1L in combination with 4-phenylbutyrate significantly improved tumor growth control in MEWO melanoma tumors, resulting in improved 92 day MOS (***$p < 0.001$ ^{212}Pb/PBA vs control; Figure 6B). Three out of seven animals survived to the conclusion of the study. Together, these data indicate that [^{212}Pb]DOTA-MC1L α-particle radiation can significantly control tumor growth in both human $BRAF^{V600E}$ and $BRAF^{WT}$ melanoma, despite the relative lower MC1R baseline level compared to B16 murine melanoma. Acute toxicity was not observed in animals that received therapies. H&E staining

of kidney samples demonstrated mild-to-mixed effects on morphology, from no significant findings to mild observable kidney injury (Figure 7). Pathology analysis of mild kidney injury was based on observations of clusters of renal tubules, which appeared mildly dilated and lined by flattened epithelial cells (black arrows), scattered tubules that contain sloughed epithelial cells (blue arrows), and glomerular sclerosis (circled) marked by multifocal scattered glomerular capillary loops.

DISCUSSION

FDA-approved MAPK-pathway-inhibiting drugs, including $BRAF_i$ and MEK_i, are targeted therapies indicated for melanoma patients whose malignancy has acquired $BRAF^{V600X}$ point mutations (primarily $BRAF^{V600E}$). Two available $BRAF_i$, dabrafenib and vemurafenib, were tested in this study for MAPK inhibition. HDAC inhibitors used in this study were vorinostat and 4-phenylbutyrate, both of which were class I and II HDAC inhibitors.[54] Vorinostat is a hydroxamate and has been approved by FDA for treatment of advanced cutaneous T-cell lymphoma.[55] 4-phenylbutyrate is an aliphatic-acidic $HDAC_i$ and has been FDA-approved to treat urea cycle disorders and is currently under investigation for cancer therapy, hemoglobinopathies, motor neuron diseases, and cystic fibrosis.[56] Despite the difference in chemical structures, both vorinostat and 4-phenylbutyrate inhibit HDAC I and II via direct interaction with the zinc ion at the base of the catalytic pocket.[57] Of note, HDAC inhibitors have been reported to enhance the sensitivity to ionizing radiation in cancer cells by altering the gene expression both preradiation and postradiation.[58–62] It is possible that HDAC inhibition treatments carried out in this study may have increased the sensitivity of melanoma tumors to 212Pb α-particle radio-therapy—in addition to directing increased radiation dose to the tumor microenvironment via upregulation of MC1R expression in tumors.

MC1R upregulation was analyzed in both $BRAF^{V600E}$ and $BRAF^{WT}$ cell lines using qRT-PCR, flow cytometry, and radioligand binding assays. The [^{125}I]NDP-α-MSH radioligand binding assay has long been used to measure the expression of MC1R on cell membranes.[24,25,63] Importantly, this assay is relevant to MC1R-targeted therapy because DOTA-MC1L was developed based on the MC1R native ligand (i.e., α-MSH), which shares the same binding sequence domain with [^{125}I]NDP-α-MSH. Our data also suggest that the transcription factor MITF plays a key role in regulating the pharmacological induction of MC1R expression by both $BRAF_i$ and $HDAC_i$. These results are consistent with previous investigations, which identified regulation of MC1R as linked with transcription factors CREB and MITF.[37,46,47] These studies indicate that phosphorylated CREB binds to CRE (a cAMP responsive element of the MITF promoter) and initiates MITF expression that activates the downstream synthesis of MC1R, tyrosinase, tyrosinase-related proteins 1/2, and other proteins. On the other hand, MITF transcriptional activity and stability are tightly regulated by MAPK pathway signaling. $BRAF^{V600E}$ mutation results in highly activated ERK1/2 and concomitant phosphorylation of MITF that promotes protease-mediated degradation of the MITF protein.[48,50,52,64–67] These observations provide a basis for employing MAPK inhibition as an approach to concomitantly enhance MC1R protein levels. We also found that HDAC inhibitors upregulated both MITF and MC1R expression simultaneously, ostensibly by inducing hyperacetylation of histones that drive the expression

of both *MITF* and *MC1R* genes. $HDAC_i$ are known to directly induce transcription factors such as LEF and CREB that potentially drive the expression of *MITF* and *MC1R*.[37,46,54]

For the studies presented here, all therapies were started on the same day (day 0). Interestingly, despite the relatively lower expression of MC1R in A2058 and MEWO cells compared with B16 melanoma cells, [^{212}Pb]DOTA-MC1L α-particle radiotherapy significantly slowed tumor growth rates in these preclinical models, potentially due to the highly cytotoxic ^{212}Pb α-particle emission and energy deposition in the tumor microenvironment. All [^{212}Pb]DOTA-MC1L radiotherapies in the present study were single dose, whereas ongoing studies in our laboratories are investigating multiple-dosing strategies, sustainability of pharmacologically-enhanced cell-surface MC1R expression, and tolerability of the treatments at higher doses. Interestingly, a large portion of MC1R was observed in the cytosolic area. Localization of the receptor could potentially impact the therapeutic effectiveness. A recent study demonstrated that pharmacological manipulation of the localization and distribution of the HER2 receptor improved trastuzumab binding and therapeutic efficacy.[68]

Mild nephrotoxicity was observed by the pathology analysis of select animals in this study. Kidney toxicity is a major concern for the targeted-radionuclide therapy and is managed in the clinical setting by the coinfusion of positively charged amino acids to facilitate faster renal clearance of radio-peptides.[69] The mechanism of radiopeptide retention in kidney is not fully understood, but multifunctional endocytic receptors megalin/cubilin are reported to play an important role in the process of reabsorption in the proximal tubules.[70,71] Therefore, ongoing efforts include optimizing the peptide structure and disrupting these receptors to facilitate excretion of excessive radiopeptide and reducing nephrotoxicity.

CONCLUSIONS

In this study, we report for the first time on the use of pharmacological approaches to enhance the expression of drug delivery to target protein MC1R as a means to improve therapeutic efficacy in human malignant melanoma in mice. Initial study of clinical biopsies confirms positive but heterogeneous expression of MC1R in human melanoma and suggests that the MC1R expression may increase with disease progression. MC1R expression was upregulated using BRAF and HDAC inhibitors via MITF-dependent mechanisms. The combination of MC1R-targeted radionuclide therapy and $BRAF_i$/$HDAC_i$ leads to significant tumor growth arrest and improved overall survival in both $BRAF^{V600E}$ and $BRAF^{WT}$ melanoma. Together, these findings demonstrate that the combination of MC1R-targeted therapies with FDA-approved $MAPK_i$ and $HDAC_i$ can be an effective regimen for $BRAF^{V600E}$ and $BRAF^{WT}$ melanoma.

ACKNOWLEDGMENTS

The data presented herein were obtained at the Flow Cytometry Facility, which is a Carver College of Medicine/ Holden Comprehensive Cancer Center core research facility at the University of Iowa. The facility is funded through user fees and the generous financial support of the Carver College of Medicine, Holden Comprehensive Cancer Center, and Iowa City Veteran's Administration Medical Center. Research reported in this publication was supported by the National Cancer Institute of the National Institutes of Health under award number P30CA086862. Samples and clinical data were obtained through the University of Iowa Melanoma, Skin & Ocular Repository

(MaST), an Institutional Review Board-approved biospecimen repository. This research is supported by the U.S. Department of Energy Isotope Program, managed by the Office of Science for Nuclear Physics.

Funding

This work was partially supported by the following grants: US Nuclear Regulatory Commission: NRC-HQ-84-14-FOA-0003; US National Institutes of Health: K25CA172218-01A1 (M.K.S.); 1P50CA174521-01A1 (M.K.S.); 1-S10-RR025439-01 (Cancer Center); National Center for Research Resources 1-S10-RR0125036-01 and NIH SBIR 1R43CA203430-01 (Viewpoint Molecular Targeting, Inc.).

REFERENCES

(1). Siegel RL; Miller KD; Jemal A Cancer statistics, 2017. CA Cancer J. Clin 2017, 67, 7–30. [PubMed: 28055103]

(2). Wolchok JD; Chiarion-Sileni V; Gonzalez R; Rutkowski P; Grob J-J; Cowey CL; Lao CD; Wagstaff J; Schadendorf D; Ferrucci PF; Smylie M; Dummer R; Hill A; Hogg D; Haanen J; Carlino MS; Bechter O; Maio M; Marquez-Rodas I; Guidoboni M; McArthur G; Lebbé C; Ascierto PA; Long GV; Cebon J; Sosman J; Postow MA; Callahan MK; Walker D; Rollin L; Bhore R; Hodi FS; Larkin J Overall Survival with Combined Nivolumab and Ipilimumab in Advanced Melanoma. N. Engl. J. Med 2017, 377, 1345–1356. [PubMed: 28889792]

(3). Weber J; Mandala M; Del Vecchio M; Gogas HJ; Arance AM; Cowey CL; Dalle S; Schenker M; Chiarion-Sileni V; Marquez-Rodas I; Grob J-J; Butler MO; Middleton MR; Maio M; Atkinson V; Queirolo P; Gonzalez R; Kudchadkar RR; Smylie M; Meyer N; Mortier L; Atkins MB; Long GV; Bhatia S; Lebbé C; Rutkowski P; Yokota K; Yamazaki N; Kim TM; de Pril V; Sabater J; Qureshi A; Larkin J; Ascierto PA; CheckMate C Adjuvant Nivolumab versus Ipilimumab in Resected Stage III or IV Melanoma. N. Engl. J. Med 2017, 377, 1824–1835. [PubMed: 28891423]

(4). Luke JJ; Flaherty KT; Ribas A; Long GV Targeted agents and immunotherapies: optimizing outcomes in melanoma. Nat. Rev. Clin. Oncol 2017, 14, 463–482. [PubMed: 28374786]

(5). Jenkins RW; Barbie DA; Flaherty KT Mechanisms of resistance to immune checkpoint inhibitors. Br. J. Cancer 2018, 118, 9–16. [PubMed: 29319049]

(6). Sharma P; Hu-Lieskovan S; Wargo JA; Ribas A Primary, Adaptive, and Acquired Resistance to Cancer Immunotherapy. Cell 2017, 168, 707–723. [PubMed: 28187290]

(7). Restifo NP; Smyth MJ; Snyder A Acquired resistance to immunotherapy and future challenges. Nat. Rev. Cancer 2016, 16, 121–126. [PubMed: 26822578]

(8). Pitt JM; Vétizou M; Daillére R; Roberti MP; Yamazaki T; Routy B; Lepage P; Boneca IG; Chamaillard M; Kroemer G; Zitvogel L Resistance Mechanisms to Immune-Checkpoint Blockade in Cancer: Tumor-Intrinsic and -Extrinsic Factors. Immunity 2016, 44, 1255–1269. [PubMed: 27332730]

(9). Hugo W; Shi H; Sun L; Piva M; Song C; Kong X; Moriceau G; Hong A; Dahlman KB; Johnson DB; Sosman JA; Ribas A; Lo RS Non-genomic and Immune Evolution of Melanoma Acquiring MAPKi Resistance. Cell 2015, 162, 1271–1285. [PubMed: 26359985]

(10). Van Allen EM; Wagle N; Sucker A; Treacy DJ; Johannessen CM; Goetz EM; Place CS; Taylor-Weiner A; Whittaker S; Kryukov GV; Hodis E; Rosenberg M; McKenna A; Cibulskis K; Farlow D; Zimmer L; Hillen U; Gutzmer R; Goldinger SM; Ugurel S; Gogas HJ; Egberts F; Berking C; Trefzer U; Loquai C; Weide B; Hassel JC; Gabriel SB; Carter SL; Getz G; Garraway LA; Schadendorf D The Genetic Landscape of Clinical Resistance to RAF Inhibition in Metastatic Melanoma. Cancer Discov 2014, 4, 94–109. [PubMed: 24265153]

(11). Rizos H; Menzies AM; Pupo GM; Carlino MS; Fung C; Hyman J; Haydu LE; Mijatov B; Becker TM; Boyd SC; Howle J; Saw R; Thompson JF; Kefford RF; Scolyer RA; Long GV BRAF inhibitor resistance mechanisms in metastatic melanoma: spectrum and clinical impact. Clin. Cancer Res 2014, 20, 1965–1977. [PubMed: 24463458]

(12). Kugel CH 3rd; Aplin AE Adaptive resistance to RAF inhibitors in melanoma. Pigment Cell Melanoma Res 2014, 27, 1032–1038. [PubMed: 24828387]

(13). Johannessen CM; Johnson LA; Piccioni F; Townes A; Frederick DT; Donahue MK; Narayan R; Flaherty KT; Wargo JA; Root DE; Garraway LA A melanocyte lineage program confers resistance to MAP kinase pathway inhibition. Nature 2013, 504, 138–142. [PubMed: 24185007]

(14). Shi H; Moriceau G; Kong X; Lee MK; Lee H; Koya RC; Ng C; Chodon T; Scolyer RA; Dahlman KB; Sosman JA; Kefford RF; Long GV; Nelson SF; Ribas A; Lo RS Melanoma whole-exome sequencing identifies (V600E)B-RAF amplification-mediated acquired B-RAF inhibitor resistance. Nat. Commun 2012, 3, 724. [PubMed: 22395615]

(15). Villanueva J; Vultur A; Herlyn M Resistance to BRAF inhibitors: unraveling mechanisms and future treatment options. Cancer Res 2011, 71, 7137–7140. [PubMed: 22131348]

(16). Rodrik-Outmezguine VS; Chandarlapaty S; Pagano NC; Poulikakos PI; Scaltriti M; Moskatel E; Baselga J; Guichard S; Rosen N mTOR kinase inhibition causes feedback-dependent biphasic regulation of AKT signaling. Cancer Discov 2011, 1, 248–259. [PubMed: 22140653]

(17). Poulikakos PI; Persaud Y; Janakiraman M; Kong X; Ng C; Moriceau G; Shi H; Atefi M; Titz B; Gabay MT; Salton M; Dahlman KB; Tadi M; Wargo JA; Flaherty KT; Kelley MC; Misteli T; Chapman PB; Sosman JA; Graeber TG; Ribas A; Lo RS; Rosen N; Solit DB RAF inhibitor resistance is mediated by dimerization of aberrantly spliced BRAF(V600E). Nature 2011, 480, 387–390. [PubMed: 22113612]

(18). Shoushtari AN; Friedman CF; Navid-Azarbaijani P; Postow MA; Callahan MK; Momtaz P; Panageas KS; Wolchok JD; Chapman PB Measuring Toxic Effects and Time to Treatment Failure for Nivolumab Plus Ipilimumab in Melanoma. JAMA Oncol 2018, 4, 98–101. [PubMed: 28817755]

(19). Schadendorf D; Wolchok JD; Hodi FS; Chiarion-Sileni V; Gonzalez R; Rutkowski P; Grob J-J; Cowey CL; Lao CD; Chesney J; Robert C; Grossmann K; McDermott D; Walker D; Bhore R; Larkin J; Postow MA Efficacy and Safety Outcomes in Patients With Advanced Melanoma Who Discontinued Treatment With Nivolumab and Ipilimumab Because of Adverse Events: A Pooled Analysis of Randomized Phase II and III Trials. J. Clin. Oncol 2017, 35, 3807–3814. [PubMed: 28841387]

(20). Hassel JC; Heinzerling L; Aberle J; Bähr O; Eigentler TK; Grimm M-O; Grünwald V; Leipe J; Reinmuth N; Tietze JK; Trojan J; Zimmer L; Gutzmer R Combined immune checkpoint blockade (anti-PD-1/anti-CTLA-4): Evaluation and management of adverse drug reactions. Cancer Treatment Rev 2017, 57, 36–49.

(21). Weber JS; Yang JC; Atkins MB; Disis ML Toxicities of Immunotherapy for the Practitioner. J. Clin. Oncology 2015, 33, 2092–2099.

(22). Rosenkranz AA; Slastnikova TA; Durymanov MO; Sobolev AS Malignant melanoma and melanocortin 1 receptor. Biochemistry 2013, 78, 1228–1237. [PubMed: 24460937]

(23). Salazar-Onfray F; López M; Lundqvist A; Aguirre A; Escobar A; Serrano A; Korenblit C; Petersson M; Chhajlani V; Larsson O; Kiessling R Tissue distribution and differential expression of melanocortin 1 receptor, a malignant melanoma marker. Br. J. Cancer 2002, 87, 414–422. [PubMed: 12177778]

(24). Tatro JB; Atkins M; Mier JW; Hardarson S; Wolfe H; Smith T; Entwistle ML; Reichlin S Melanotropin receptors demonstrated in situ in human melanoma. J. Clin. Invest 1990, 85, 1825–1832. [PubMed: 2347915]

(25). Siegrist W; Solca F; Stutz S; Giuffré L; Carrel S; Girard J; Eberle AN Characterization of receptors for alpha-melanocyte-stimulating hormone on human melanoma cells. Cancer Res 1989, 49, 6352–6358. [PubMed: 2804981]

(26). Ghanem GE; Comunale G; Libert A; Vercammen-Grandjean A; Lejeune FJ Evidence for alpha-melanocyte-stimulating hormone (α-MSH) receptors on human malignant melanoma cells. Int. J. Cancer 1988, 41, 248–255. [PubMed: 2828246]

(27). Martin ME; Sue O'Dorisio M; Leverich WM; Kloepping KC; Walsh SA; Schultz MK ″Click″-Cyclized 68Ga-Labeled Peptides for Molecular Imaging and Therapy: Synthesis and Preliminary In Vitro and In Vivo Evaluation in a Melanoma Model System. Recent Results Cancer Res 2013, 194, 149–175. [PubMed: 22918759]

(28). Guo H; Yang J; Gallazzi F; Miao Y Reduction of the Ring Size of Radiolabeled Lactam Bridge-Cyclized -MSH Peptide, Resulting in Enhanced Melanoma Uptake. J. Nucl. Med 2010, 51, 418–426. [PubMed: 20150256]

(29). Cantorias MV; Figueroa SD; Quinn TP; Lever JR; Hoffman TJ; Watkinson LD; Carmack TL; Cutler CS Development of high-specific-activity 68Ga-labeled DOTA-rheniumcyclized α-MSH peptide analog to target MC1 receptors overex-pressed by melanoma tumors. Nucl. Med. Biol 2009, 36, 505–513. [PubMed: 19520291]

(30). Miao Y; Figueroa SD; Fisher DR; Moore HA; Testa RF; Hoffman TJ; Quinn TP 203Pb-labeled alpha-melanocyte-stimulating hormone peptide as an imaging probe for melanoma detection. J. Nucl. Med 2008, 49, 823–829. [PubMed: 18413404]

(31). Miao Y; Hylarides M; Fisher DR; Shelton T; Moore H; Wester DW; Fritzberg AR; Winkelmann CT; Hoffman T; Quinn TP Melanoma Therapy via Peptide-Targeted -Radiation. Clin. Cancer Res 2005, 11, 5616–5621. [PubMed: 16061880]

(32). McQuade P; Miao Y; Yoo J; Quinn TP; Welch MJ; Lewis JS Imaging of Melanoma Using64Cu−and 86Y−DOTA−ReCCMSH(Arg11), a Cyclized Peptide Analogue of α-MSH. J. Med. Chem 2005, 48, 2985–2992. [PubMed: 15828837]

(33). Cheng Z; Chen J; Miao Y; Owen NK; Quinn TP; Jurisson SS Modification of the Structure of a Metallopeptide: Synthesis and Biological Evaluation of111In-Labeled DOTA-Conjugated Rhenium-Cyclized α-MSH Analogues. J. Med. Chem 2002, 45, 3048–3056. [PubMed: 12086490]

(34). Tafreshi NK; Tichacek CJ; Pandya DN; Doligalski ML; Budzevich MM; Kil H; Bhatt NB; Kock ND; Messina JL; Ruiz EE; Delva NC; Weaver A; Gibbons WR; Boulware DC; Khushalani NI; El-Haddad G; Triozzi PL; Moros EG; McLaughlin ML; Wadas T; Morse D Melanocortin 1 Receptor Targeted Alpha-Particle Therapy for Metastatic Uveal Melanoma. J. Nucl. Med 2019, DOI: 10.2967/jnumed.118.217240.

(35). Miao Y; Whitener D; Feng W; Owen NK; Chen J; Quinn TP Evaluation of the Human Melanoma Targeting Properties of Radiolabeled α-Melanocyte Stimulating Hormone Peptide Analogues. Bioconjug. Chem 2003, 14, 1177–1184. [PubMed: 14624632]

(36). Garcia-Borron JC; Sanchez-Laorden BL; Jimenez-Cervantes C Melanocortin-1 receptor structure and functional regulation. Pigment Cell Res 2005, 18, 393–410. [PubMed: 16280005]

(37). Rouzaud F; Hearing VJ Regulatory elements of the melanocortin 1 receptor. Peptides 2005, 26, 1858–1870. [PubMed: 16005546]

(38). Scott MC; Suzuki I; Abdel-Malek ZA Regulation of the human melanocortin 1 receptor expression in epidermal melanocytes by paracrine and endocrine factors and by ultraviolet radiation. Pigment Cell Res 2002, 15, 433–439. [PubMed: 12453185]

(39). Siegrist W; Eberle AN Homologous regulation of the MSH receptor in melanoma cells. J. Recept Res 1993, 13, 263–281. [PubMed: 8383755]

(40). Frederick DT; Piris A; Cogdill AP; Cooper ZA; Lezcano C; Ferrone CR; Mitra D; Boni A; Newton LP; Liu C; Peng W; Sullivan RJ; Lawrence DP; Hodi FS; Overwijk WW; Lizee G; Murphy GF; Hwu P; Flaherty KT; Fisher DE; Wargo JA BRAF inhibition is associated with enhanced melanoma antigen expression and a more favorable tumor micro-environment in patients with metastatic melanoma. Clin. Cancer Res 2013, 19, 1225–1231. [PubMed: 23307859]

(41). Rose AAN; Annis MG; Frederick DT; Biondini M; Dong Z; Kwong L; Chin L; Keler T; Hawthorne T; Watson IR; Flaherty KT; Siegel PM MAPK Pathway Inhibitors Sensitize BRAF-Mutant Melanoma to an Antibody-Drug Conjugate Targeting GPNMB. Clin. Cancer Res 2016, 22, 6088–6098. [PubMed: 27515299]

(42). Asundi J; Lacap JA; Clark S; Nannini M; Roth L; Polakis P MAPK pathway inhibition enhances the efficacy of an anti-endothelin B receptor drug conjugate by inducing target expression in melanoma. Mol. Cancer Therapeut 2014, 13, 1599–1610.

(43). Taelman VF; Radojewski P; Marincek N; Ben-Shlomo A; Grotzky A; Olariu CI; Perren A; Stettler C; Krause T; Meier LP; Cescato R; Walter MA Upregulation of Key Molecules for Targeted Imaging and Therapy. J. Nucl. Med 2016, 57, 1805–1810. [PubMed: 27363833]

(44). DuBois SG; Groshen S; Park JR; Haas-Kogan DA; Yang X; Geier E; Chen E; Giacomini K; Weiss B; Cohn SL; Granger MM; Yanik GA; Hawkins R; Courtier J; Jackson H; Goodarzian F; Shimada H; Czarnecki S; Tsao-Wei D; Villablanca JG; Marachelian A; Matthay KK Phase I Study of Vorinostat as a Radiation Sensitizer with 131I-Metaiodobenzylguanidine (131IMIBG) for Patients with Relapsed or Refractory Neuroblastoma. Clin. Cancer Res 2015, 21, 2715–2721. [PubMed: 25695691]

(45). More SS; Itsara M; Yang X; Geier EG; Tadano MK; Seo Y; Vanbrocklin HF; Weiss WA; Mueller S; Haas-Kogan DA; Dubois SG; Matthay KK; Giacomini KM Vorinostat increases expression of functional norepinephrine transporter in neuroblastoma in vitro and in vivo model systems. Clin. Cancer Res 2011, 17, 2339–2349. [PubMed: 21421857]

(46). Aoki H; Moro O Involvement of microphthalmia-associated transcription factor (MITF) in expression of human melanocortin-1 receptor (MC1R). Life Sci 2002, 71, 2171–2179. [PubMed: 12204775]

(47). Adachi S; Morii E; Kim D.-k.; Ogihara H; Jippo T; Ito A; Lee Y-M; Kitamura Y Involvement of mi-Transcription Factor in Expression of α-Melanocyte-Stimulating Hormone Receptor in Cultured Mast Cells of Mice. J. Immunol 2000, 164, 855–860. [PubMed: 10623832]

(48). Hsiao JJ; Fisher DE The roles of microphthalmia-associated transcription factor and pigmentation in melanoma. Arch. Biochem. Biophys 2014, 563, 28–34. [PubMed: 25111671]

(49). Carreira S; Goodall J; Denat L; Rodriguez M; Nuciforo P; Hoek KS; Testori A; Larue L; Goding CR Mitf regulation of Dia1 controls melanoma proliferation and invasiveness. Genes Dev 2006, 20, 3426–3439. [PubMed: 17182868]

(50). Garraway LA; Widlund HR; Rubin MA; Getz G; Berger AJ; Ramaswamy S; Beroukhim R; Milner DA; Granter SR; Du J; Lee C; Wagner SN; Li C; Golub TR; Rimm DL; Meyerson ML; Fisher DE; Sellers WR Integrative genomic analyses identify MITF as a lineage survival oncogene amplified in malignant melanoma. Nature 2005, 436, 117–122. [PubMed: 16001072]

(51). Li M; Zhang X; Quinn TP; Lee D; Liu D; Kunkel F; Zimmerman BE; McAlister D; Olewein K; Menda Y; Mirzadeh S; Copping R; Johnson FL; Schultz MK Automated cassette-based production of high specific activity [203/212 Pb]peptide-based theranostic radiopharmaceuticals for image-guided radionuclide therapy for cancer. Appl. Radiat. Isot 2017, 127, 52–60. [PubMed: 28521118]

(52). Hartman ML; Czyz M MITF in melanoma: mechanisms behind its expression and activity. Cell. Mol. Life Sci 2015, 72, 1249–1260. [PubMed: 25433395]

(53). Chen KG; Valencia JC; Lai B; Zhang G; Paterson JK; Rouzaud F; Berens W; Wincovitch SM; Garfield SH; Leapman RD; Hearing VJ; Gottesman MM Melanosomal sequestration of cytotoxic drugs contributes to the intractability of malignant melanomas. Proc. Natl. Acad. Sci. U.S.A 2006, 103, 9903–9907. [PubMed: 16777967]

(54). Xu WS; Parmigiani RB; Marks PA Histone deacetylase inhibitors: molecular mechanisms of action. Oncogene 2007, 26, 5541–5552. [PubMed: 17694093]

(55). Mann BS; Johnson JR; Cohen MH; Justice R; Pazdur R FDA approval summary: vorinostat for treatment of advanced primary cutaneous T-cell lymphoma. Oncologist 2007, 12, 1247–1252. [PubMed: 17962618]

(56). Iannitti T; Palmieri B Clinical and experimental applications of sodium phenylbutyrate. Drugs R D 2011, 11, 227–249. [PubMed: 21902286]

(57). Finnin MS; Donigian JR; Cohen A; Richon VM; Rifkind RA; Marks PA; Breslow R; Pavletich NP Structures of a histone deacetylase homologue bound to the TSA and SAHA inhibitors. Nature 1999, 401, 188–193. [PubMed: 10490031]

(58). Pont LM; Naipal K; Kloezeman JJ; Venkatesan S; van den Bent M; van Gent DC; Dirven CM; Kanaar R; Lamfers ML; Leenstra S DNA damage response and anti-apoptotic proteins predict radiosensitization efficacy of HDAC inhibitors SAHA and LBH589 in patient-derived glioblastoma cells. Cancer Lett 2015, 356, 525–535. [PubMed: 25305451]

(59). Shi W; Lawrence YR; Choy H; Werner-Wasik M; Andrews DW; Evans JJ; Judy KD; Farrell CJ; Moshel Y; Berger AC; Bar-Ad V; Dicker AP Vorinostat as a radiosensitizer for brain metastasis: a phase I clinical trial. J. Neurooncol 2014, 118, 313–319. [PubMed: 24728831]

(60). Hehlgans S; Storch K; Lange I; Cordes N The novel HDAC inhibitor NDACI054 sensitizes human cancer cells to radiotherapy. Radiother. Oncol 2013, 109, 126–132. [PubMed: 24060178]

(61). Groselj B; Sharma NL; Hamdy FC; Kerr M; Kiltie AE Histone deacetylase inhibitors as radiosensitisers: effects on DNA damage signalling and repair. Br. J. Cancer 2013, 108, 748–754. [PubMed: 23361058]

(62). Chinnaiyan P; Cerna D; Burgan WE; Beam K; Williams ES; Camphausen K; Tofilon PJ Postradiation sensitization of the histone deacetylase inhibitor valproic acid. Clinical Cancer Res 2008, 14, 5410–5415. [PubMed: 18765532]

(63). Wong W; Minchin RF Binding and internalization of the melanocyte stimulating hormone receptor ligand [Nle4, d-Phe7]α-MSH in B16 melanoma cells. Int. J. Biochem. Cell Biol 1996, 28, 1223–1232. [PubMed: 9022281]

(64). Smith MP; Brunton H; Rowling EJ; Ferguson J; Arozarena I; Miskolczi Z; Lee JL; Girotti MR; Marais R; Levesque MP; Dummer R; Frederick DT; Flaherty KT; Cooper ZA; Wargo JA; Wellbrock C Inhibiting Drivers of Non-mutational Drug Tolerance Is a Salvage Strategy for Targeted Melanoma Therapy. Cancer Cell 2016, 29, 270–284. [PubMed: 26977879]

(65). Wellbrock C; Arozarena I Microphthalmia-associated transcription factor in melanoma development and MAP-kinase pathway targeted therapy. Pigment Cell Melanoma Res 2015, 28, 390–406. [PubMed: 25818589]

(66). Wellbrock C; Rana S; Paterson H; Pickersgill H; Brummelkamp T; Marais R Oncogenic BRAF regulates melanoma proliferation through the lineage specific factor MITF. PLoS One 2008, 3, No. e2734. [PubMed: 18628967]

(67). Saha B; Singh SK; Sarkar C; Bera R; Ratha J; Tobin DJ; Bhadra R Activation of the Mitf promoter by lipid-stimulated activation of p38-stress signalling to CREB. Pigment Cell Res 2006, 19, 595–605. [PubMed: 17083486]

(68). Pereira PMR; Sharma SK; Carter LM; Edwards KJ; Pourat J; Ragupathi A; Janjigian YY; Durack JC; Lewis JS Caveolin-1 mediates cellular distribution of HER2 and affects trastuzumab binding and therapeutic efficacy. Nat. Commun 2018, 9, 5137. [PubMed: 30510281]

(69). DePalatis LR; Frazier KA; Cheng RC; Kotite NJ Lysine reduces renal accumulation of radioactivity associated with injection of the [177Lu]alpha-[2-(4-aminophenyl) ethyl]-1,4,7,10-tetraaza-cyclodecane-1,4,7,10-tetraacetic acid-CC49 Fab radioimmunoconjugate. Cancer Res 1995, 55, 5288–5295. [PubMed: 7585590]

(70). de Jong M; Barone R; Krenning E; Bernard B; Melis M; Visser T; Gekle M; Willnow TE; Walrand S; Jamar F; Pauwels S Megalin is essential for renal proximal tubule reabsorption of (111)In-DTPA-octreotide. J. Nucl. Med 2005, 46, 1696–1700. [PubMed: 16204720]

(71). Vegt E; van Eerd JEM; Eek A; Oyen WJG; Wetzels JFM; de Jong M; Russel FGM; Masereeuw R; Gotthardt M; Boerman OC Reducing renal uptake of radiolabeled peptides using albumin fragments. J. Nucl. Med 2008, 49, 1506–1511. [PubMed: 18703613]

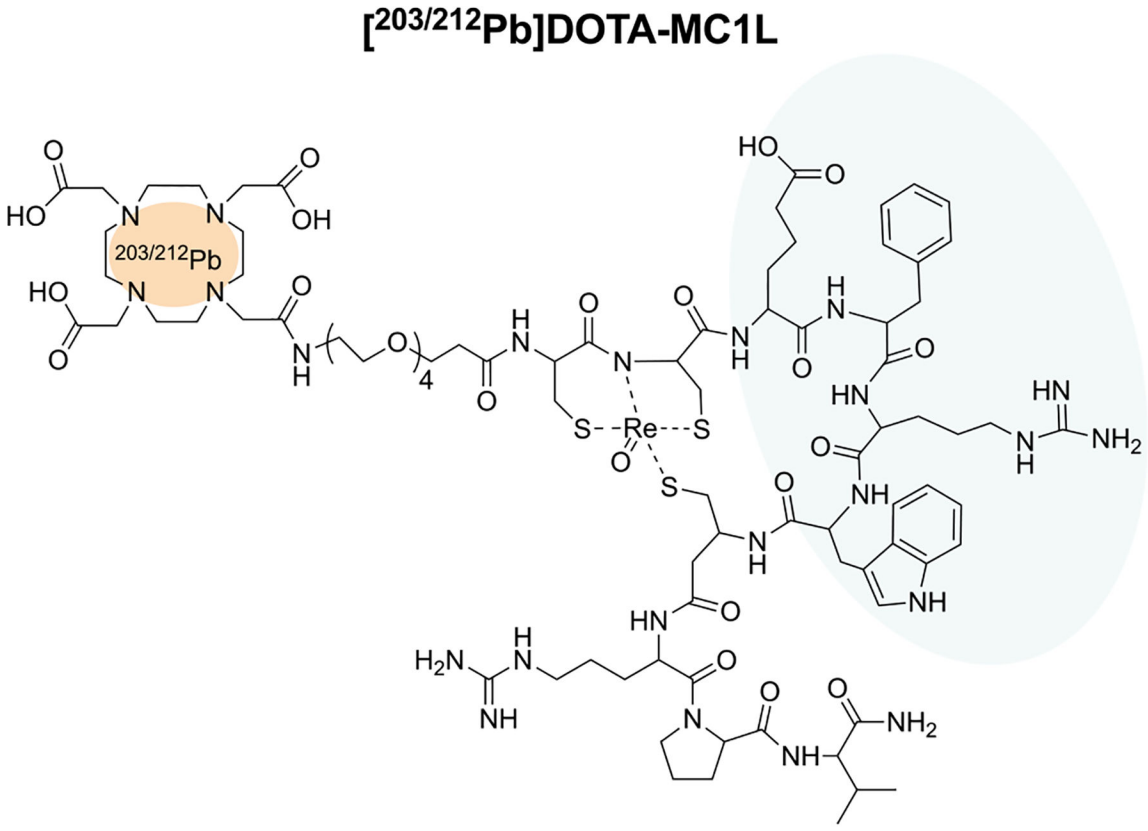

Figure 1.

MC1R-targeted ligands DOTA-MC1L. [$^{203/212}$Pb]DOTA-MC1L shares the His-D-Phe-Arg-Trp sequence (blue) moiety for receptor binding and is labeled with $^{203/212}$Pb radionuclides (red). γ emitter ^{203}Pb was used for SPECT/CT imaging, and α-particle emitter ^{212}Pb was applied for α-radiation therapy.

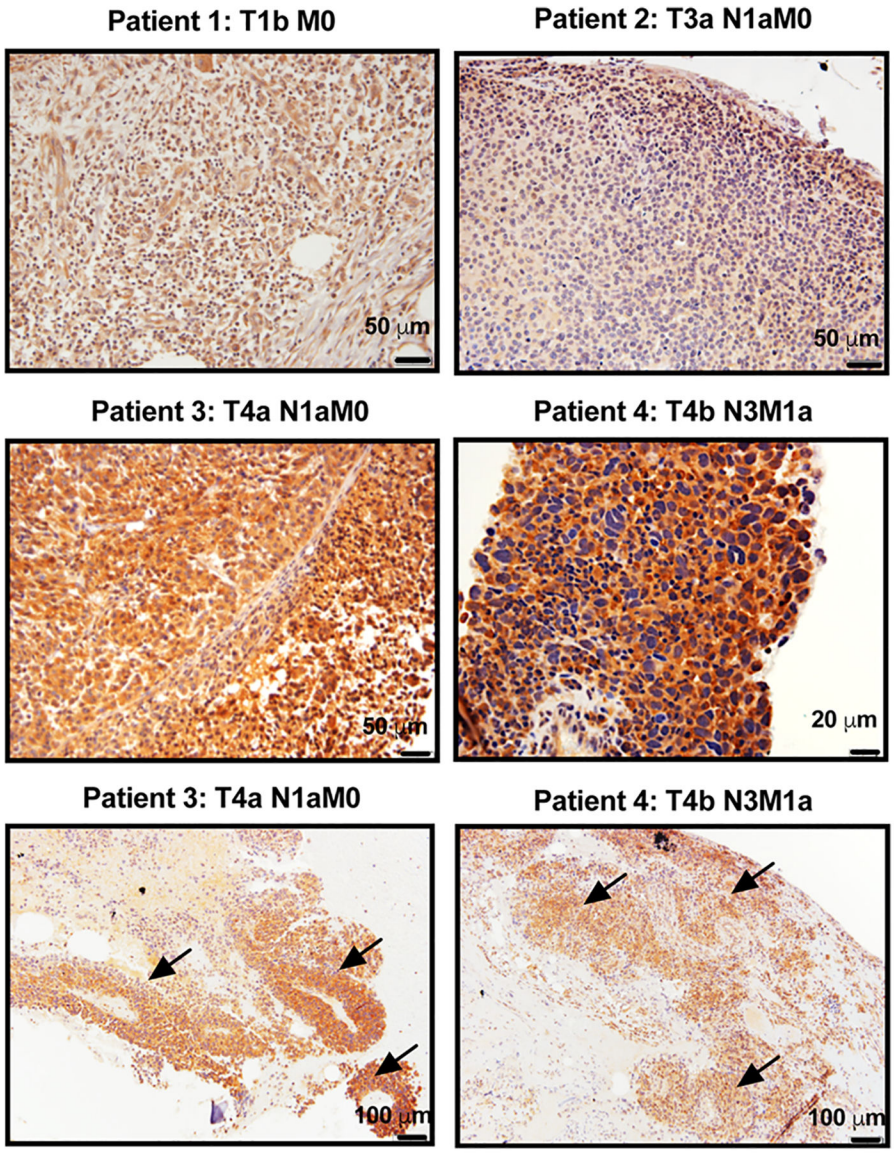

Figure 2.

IHC staining of MC1R in selected de-identified melanoma biopsies collected from human subjects. Mixed levels of MC1R expression was observed. Significantly higher expression was found in stage 4 tumors. Arrows indicate melanoma lesions observed within the adjacent normal tissue.

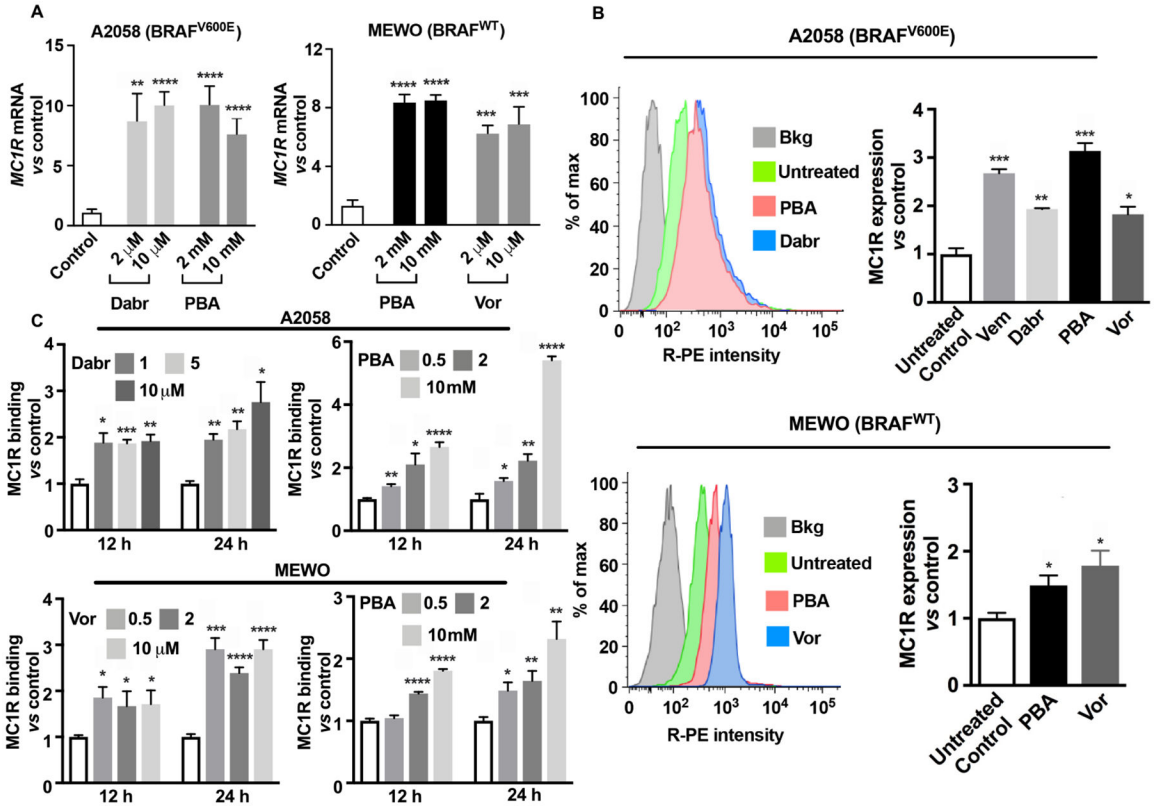

Figure 3.

MC1R expression is upregulated in human melanoma cells upon treatment with $BRAF_i$ and $HDAC_i$. (A) qRT-PCR analysis of *MC1R* mRNA expression in $BRAF^{V600E}$ A2058 cells after 24 h of incubation with $BRAF_i$ dabrafenib (Dabr) and $HDAC_i$ 4-phenylbutyrate (PBA) and in $BRAF^{WT}$ MEWO cells after 24 h treatment with $HDAC_i$ PBA and vorinostat (Vor) ($n = 3$). Data are presented as normalized mean *MC1R* mRNA ± SEM; *$p < 0.05$, **$p < 0.01$, ***$p < 0.001$, and ****$p < 0.0001$ vs controls; (B) flow cytometry histograms and protein expression of MC1R in A2058 cells after 24 h treatment with $BRAF_i$: Vem (5 μM) and Dabr (2 μM); $HDAC_i$: PBA (2 mM) and Vor (2 μM); and in MEWO cells after incubation with PBA (2 mM) and Vor (2 μM). Experiments were conducted in triplicate. Data are expressed as relative expression of MC1R vs isotype control (mean ± SEM; *$p < 0.05$, **$p < 0.01$, ***$p < 0.001$ vs controls); (C) MC1R binding with [^{125}I]NDP-α-MSH in A2058 and MEWO cells following incubation with Dabr (1−10 μM), Vor (0.5−10 μM), and PBA (0.5−10 mM) for 12−24 h ($n = 4$). Data are expressed as MC1R-ligand binding vs dimethyl sulfoxide (DMSO)-treated cells (mean ± SEM; *$p < 0.05$, **$p < 0.01$, ***$p < 0.001$, ****$p < 0.0001$ vs controls); all experiments were performed in duplicate ($n = 2$).

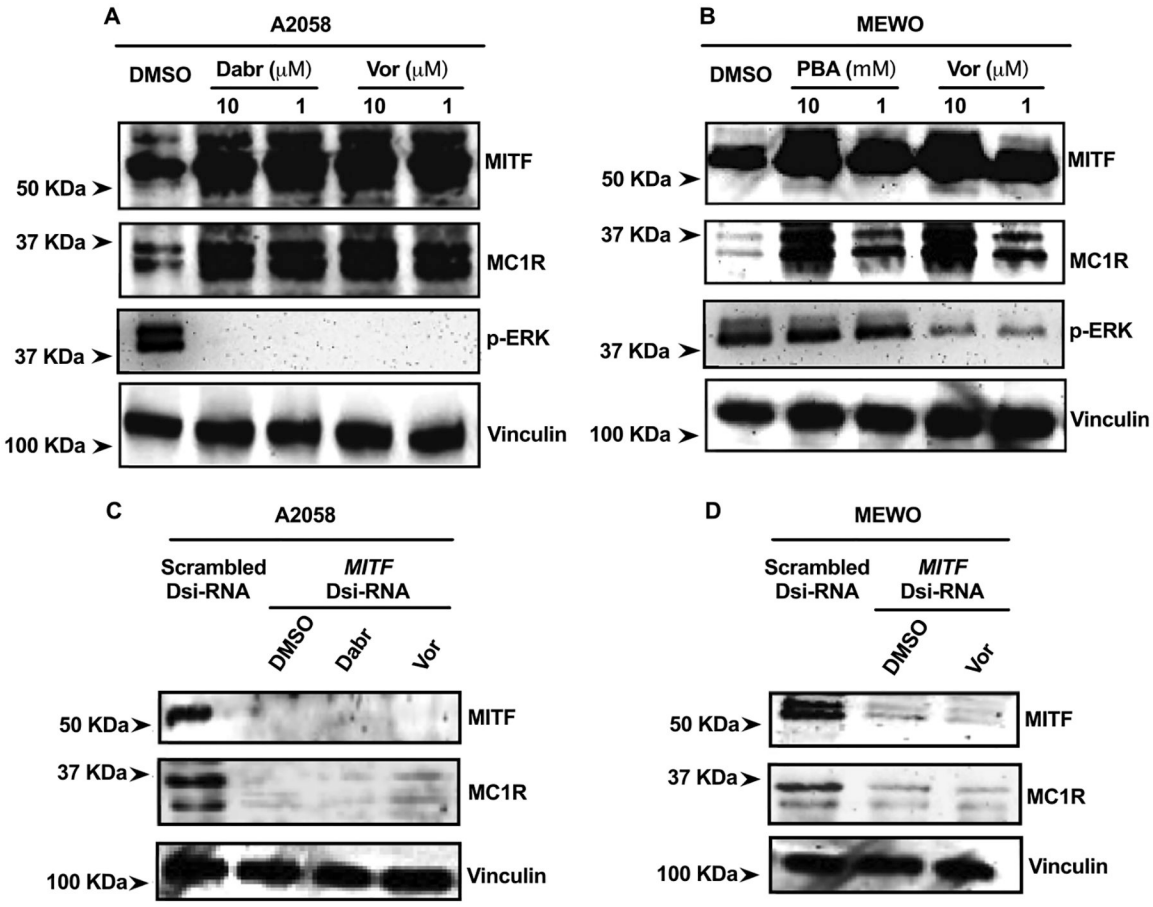

Figure 4.

Upregulation of MC1R in melanoma cells is mediated by the transcription factor MITF. Immunoblotting analysis of MC1R and MITF expressions in (A) $BRAF^{V600E}$ cells (A2058) following 24 h incubation with dabrafenib (Dabr) (1−10 μM) and vorinostat (Vor) (1−10 μM) and in (B) $BRAF^{WT}$ cells (MEWO) following 24 h exposure to HDACi vorinostat (Vor) (1−10 μM) and 4-phenylbutyrate (PBA) (1−10 mM); immunoblotting analysis of MC1R in (C) A2058 and (D) MEWO cells in response to 24 h incubation with Dabr (1 μM), Vor (1 μM), or PBA (1 mM), with normal MITF expression (negative scrambled Dsi-RNA) and attenuated MITF expression (MITF Dsi-RNA). All experiments were conducted in duplicate ($n = 2$).

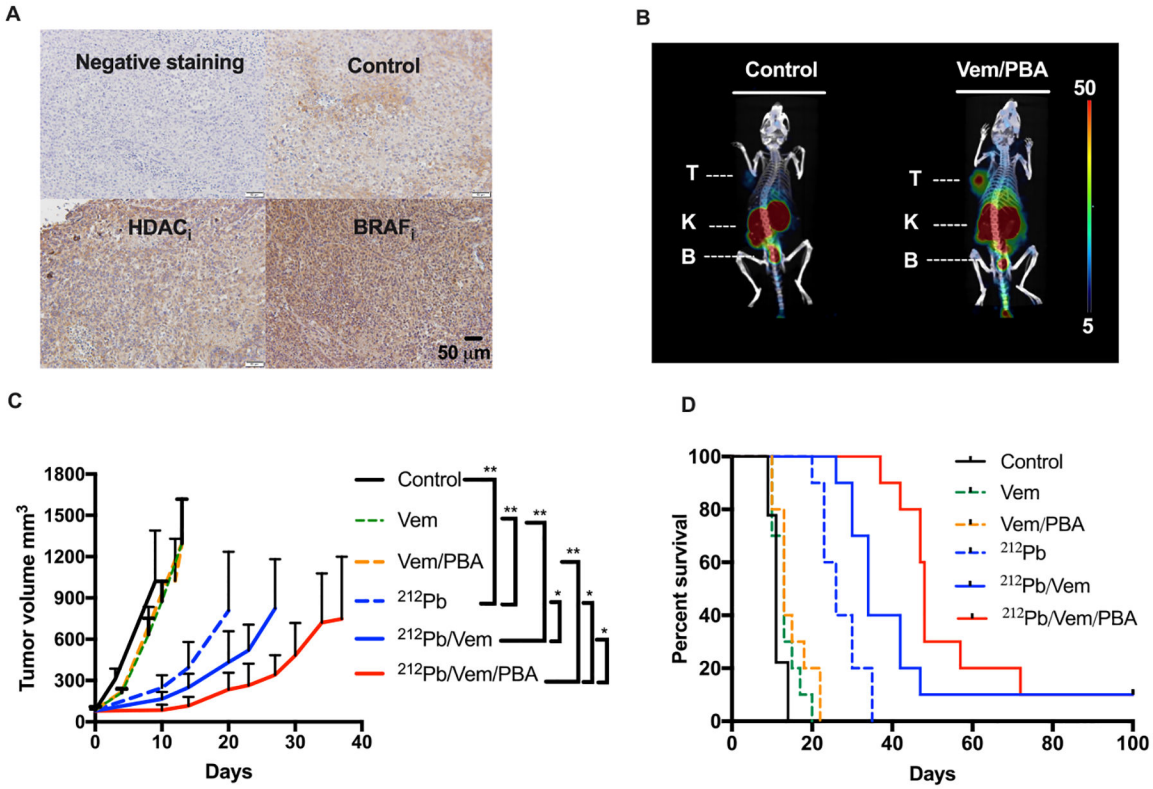

Figure 5.

Combination of BRAF, HDAC inhibitors, and MC1R-targeted ^{212}Pb α-particle therapy significantly impairs BRAF^{V600E} melanoma A2058 tumor growth and improves survival. (A) Representative IHC staining of MC1R in A2058 melanoma-bearing animals that were treated with HDAC$_i$ PBA (90 mg kg^{-1}, i.p., q.d.), BRAF$_i$ vemubrafenib (10 mg kg^{-1}, p.o., b.i.d.) ($n = 2$); (B) 2 h postinjection SPECT/CT imaging of A2058 melanoma in athymic nu/nu mice treated with vemurafenib (Vem 10 mg kg^{-1}, p.o.) and 4-phenylbutyrate (PBA 90 mg kg^{-1}, i.p.) using [^{203}Pb]DOTA-MC1L as the imaging tracer. Organs of interest are indicated as T (tumor), K (kidney), and B (bladder); (C) average tumor volume for each group of animals after treatments were initiated; data are expressed as mean ± SD; statistical analysis: *$p < 0.05$, **$p < 0.01$; (D) overall fractional survival in each treatment cohort over 100 days ($n = 9$−10 per group): vemurafenib (Vem) (10 mg kg^{-1}, p.o., b.i.d.), 4-phenylbutyrate (PBA) (90 mg kg^{-1}, i.p. q.d.), and ^{212}Pb α-particle therapy (^{212}Pb) (single dose of 5.2 MBq [^{212}Pb]DOTA-MC1L). Statistical analysis: ****$p < 0.0001$ ^{212}Pb versus control; ****$p < 0.0001$ ^{212}Pb versus Vem; **$p < 0.01$ ^{212}Pb/Vem vs ^{212}Pb; **$p < 0.01$ ^{212}Pb/Vem/PBA vs ^{212}Pb/Vem.

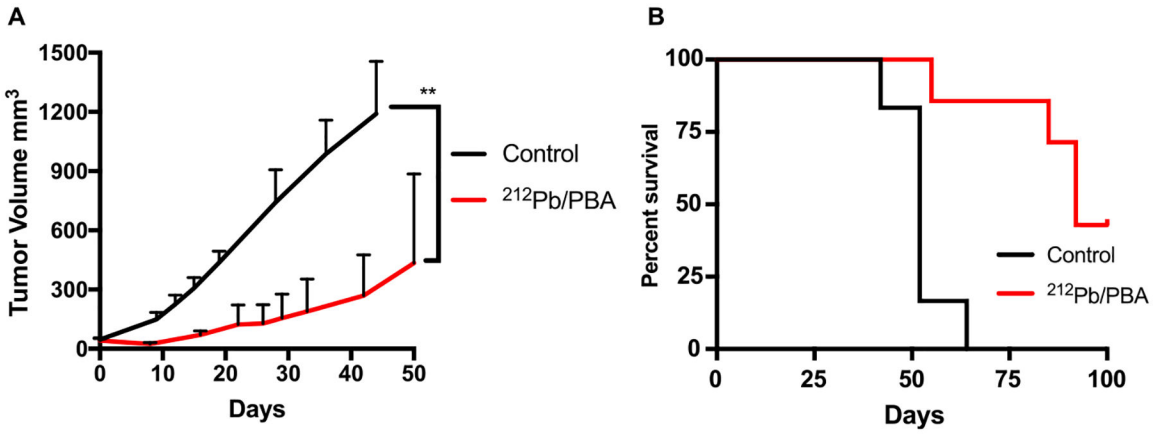

Figure 6.

Combination of HDAC inhibitor and ^{212}Pb α-particle therapy significantly slows the progression of BRAF wild-type MEWO melanoma and improves survival. (A) Average tumor volume for each group of animals after treatments were initiated; data are expressed as mean ± SD; statistical analysis: $^{**}p < 0.01$ ^{212}Pb/PBA vs control and (B) overall fractional survival in MEWO tumor xenograft models that received ^{212}Pb α-particle therapy (single dose of 5.2 MBq [^{212}Pb]DOTA-MC1L) and phenylbutyrate (^{212}Pb/PBA) (90 mg kg $^{-1}$, i.p. q.d.) ($n = 6–7$ per group; $^{***}p < 0.001$ ^{212}Pb/PBA vs control).

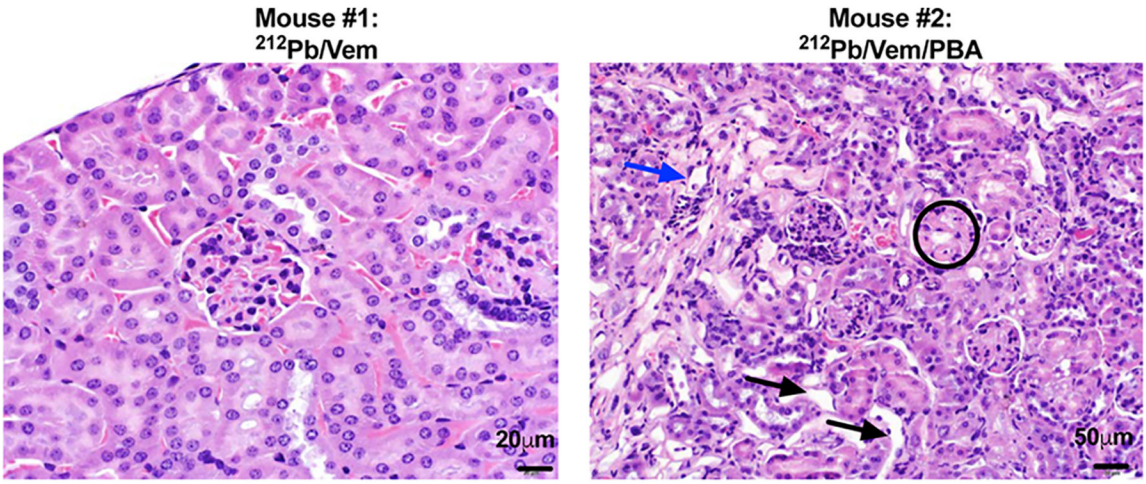

Figure 7.

Mixed level of nephrotoxicity after MC1R-targeted α-radiation therapy. No acute toxicity related to treatments was observed. Kidney samples were collected from survived animals at the conclusion of the study and stained with H&E to analyze kidney cell morphology. Nonsignificant (N.S.) to moderate nephritis was observed; black arrows: mildly dilated renal tubules lined by flattened epithelial cells; blue arrows: scattered tubules contain sloughed epithelial cells; circled: glomerular sclerosis with multifocal scattered glomerular capillary loops.